RSC Advances

PAPER

View Article Online
View Journal | View Issue

Cite this: *RSC Adv.*, 2025, **15**, 49948

APTES derived polymer with naphthalimide pendant for the fluorescent sensing of picric acid

Sithara Soman[a] and Kala R *[ab]

A fluorescent polymer based on silane was synthesised through the functionalization of 4-bromo-1,8-naphthalic anhydride with Aminopropyltriethoxysilane (APTES), followed by polycondensation (referred to as NI@SiP). Subsequently, substitution at the fourth position with *N*,*N*-dimethyl ethylene diamine, led to significant enhancement in the weak fluorescence of the NI@SiP, resulting in the polymer, FNI@SiP. Characterization of the polymer material was conducted using FTIR, FESEM, UV-vis, and fluorescent spectroscopy. FNI@SiP displayed improved solubility along with solvent-dependent fluorescence behaviour. Functionalization at the fourth position of the naphthalimide ring enhanced the fluorescence properties of the material, yielding a quantum yield of approximately 23%. The material exhibited quantitative response towards Picric acid (2,4,6-trinitrophenol denoted as TNP) at micromolar levels by fluorescence quenching in the range 1.7×10^{-6} M to 2.7×10^{-4} M, with a limit of detection value 2.63×10^{-8} M, in aqueous media. The quenching mechanism was further elucidated through time-resolved fluorescence decay measurement, revealing a mixed mechanism involved. Furthermore, a thin film polymer sensor was fabricated, leveraging the silane functionality within the polymer, enabling detection of nitroaromatics, thereby presenting new opportunities for practical application.

Received 22nd May 2025
Accepted 6th November 2025

DOI: 10.1039/d5ra03588k

rsc.li/rsc-advances

Introduction

Nitroaromatics, extensively utilized in explosives, dyes, and pesticides, pose significant environmental risks due to their toxicity and resistance to degradation, resulting in irreversible damage to soil and water in war zones and industrial areas. Developing rapid, real-time monitoring and on-site detection methods for such substances is crucial for security and environmental monitoring purposes, particularly focusing on 2,4,6-trinitrotoluene (TNT); 2,4-dinitrotoluene (DNT); and 2,4,6-trinitrophenol (TNP), commonly found in military ammunition and unexploded landmines worldwide.[1–3]

Traditionally nitroaromatics detection methods include instrumental analysis and chemical reagent detection, such as mass spectrometry, surface-enhanced Raman spectroscopy (SERS), ion mobility spectrometry (IMS), cyclic voltammetry, gas chromatography, and nuclear quadrupole resonance (NQR). However, these methods are often costly, time-consuming, and lack portability for real-time application, prompting the need for simpler, cost-effective, and more sensitive detection methods, including colorimetric and fluorescent receptors based on various materials. Fluorescence detection technology is particularly promising due to its high sensitivity, specificity, rapid response, and contactless detection capability.[4–6]

Recently, various fluorescent probes have emerged for the rapid detection of trace amounts of nitroaromatic compounds (NACs) through fluorescence quenching methods. Small molecule fluorophores, conjugated polymer nanoparticles, other fluorescent nanoparticles can be employed for this purpose.

Fluorescent polymers, among other materials, are intriguing for fluorescence-based rapid detection due to their significant signal amplification potential, arising from phenomena like the molecular wire effect. Naphthalimide-based receptors have garnered attention for their optical and photophysical properties, making them suitable for chemosensor development.[7–9]

Functionalization of naphthalimide-based polymers with silanes, particularly 3-aminopropyltriethoxysilane (APTES), offers advantages such as solubility, film formation ability, and ease of functionalization. Immobilizing receptors onto inorganic mesoporous materials, like silica nanoparticles, presents advantages in terms of sensitivity, ease of preparation, and recyclability.[10–12]

Recent studies have introduced novel chemosensors utilizing silicon-based systems, such as fluorescein-functionalized silica nanoparticles for imaging Cu^{2+} in living cells and fluoride anion sensing polymers incorporating naphthalimide signal moieties. These advancements demonstrate the potential of silane-based polymers with naphthalimide substituents for sensing applications, particularly in detecting nitroaromatics.[10,13,14]

In our study, we focused on developing a silane-based polymer with a naphthalimide substituent and functionalizing the

[a]*Department of Applied Chemistry, Cochin University of Science and Technology, Kerala, 682022, India. E-mail: kala@cusat.ac.in*

[b]*Inter University Centre for Nanomaterials and Devices (IUCND), Cochin University of Science and Technology, Kerala, 682022, India*

naphthalimide unit at the 4th position to enhance its affinity towards nitroaromatics. To the best of our knowledge no similar systems are reported towards TNP detection.

Materials and methods

Chemicals and reagents

All reagents were commercially available and used without further purification. 4-bromo-1,8-naphthalic anhydride (NA), *N*,*N*-dimethylethylenediamine, aminopropyltriethoxysilane (APTES), nitrobenzene (NB), 3,5-dinitrosalicylic acid (DNSA), 2-nitrophenol (NP), nitroethane (NE), 4-nitrobenzoic acid (NBA), 4-nitrobenzaldehyde (NBAL), and 2,3-dinitrobenzene (DNB) were purchased from Sigma-Aldrich. All solvents used were of UV grade and purchased from Spectrochem. Deionized water was used for the preparation of all solutions for the analyses.

Instrumental methods

The materials synthesised were characterised by Fourier Transform Infrared spectroscopy (JASCO FT-IR-5300 spectrometer) using KBr pellets. The surface morphology of the material was determined using SEM (Jeol JSM-6390LV/JED-2300) and TEM (HR-TEM Jeol/JEM 2100) imaging. To analyse the elemental composition of the material, CHNS analyser was used (Elementar Vario ELIII CHNS analyser). Thermogravimetric analyses were done using a Metler 851 Model SDTA/TGA instrument at a heating rate 20 °C min^{-1}. X-ray photoelectron spectroscopic analysis was carried out using PHI 5000 Versa probe Scanning Esca Microprobe.

UV-visible absorption studies were conducted using an Evolution 201 UV-visible spectrometer, covering the range from 200 to 800 nm. Measurements were performed at room temperature (298 K) in a square-shaped quartz cuvette with a path length of 10 mm.

Steady-state luminescence experiments were carried out using a Horiba Fluorolog 3 (FL-1057) spectrofluorometer. A four-face transparent quartz cuvette was utilized, with excitation and emission slit widths set at 2 nm.

Time-resolved fluorescence decay measurements were recorded on the same Horiba Fluorolog 3 instrument using time-correlated single photon counting (TCSPC). A 370 nm nano-LED with a pulse repetition rate of 100 MHz was used for excitation, and emission decay traces were collected with emission wavelength fixed at 530 nm. Multi-exponential decay analysis was performed using DAS6 software with a tri-exponential decay model.

Experimental

Synthesis of NI@SiM

The functionalization process involved the reaction of 4-bromo-1,8-naphthalic anhydride (NA) with aminopropyltriethoxysilane (APTES) in equimolar quantities (1 mmol each) under reflux conditions in dry ethanol for 4 hours, as per established literature protocols.[15] The progress of the reaction was monitored using Thin Layer Chromatography (TLC). Unreacted APTES was removed by washing with ethanol. The resulting yellow-colored product was collected, and dried.

Polymerization of NI@SiM to form NI@SiP

Subsequently, for the preparation of the polymer, the NI@SiM (1 g) was transferred into an RB flask containing 60 mL of ethanol, and 12 mL of ammonia solution was added into it. The mixture was stirred at room temperature for 12 hours, and the resulting polymer was collected, washed with ethanol, and dried.[15] The proposed structure of the material and the synthesis process are illustrated in Scheme 1. The polymer, denoted as NI@SiP, exhibited weak fluorescence when dispersed in water.

Functionalization of NI@SiP

In the subsequent step, the polymer NI@SiP was treated with *N*,*N*-dimethylethylenediamine to substitute bromine at the 4th position of the naphthalimide unit. For this, NI@SiP (1 g) was reacted with 5 mL *N*,*N*-dimethylethylenediamine at 130 °C and the product obtained was collected. Purification of the polymer was done by dissolving the polymer in DCM, and washing the organic layer several times with dil. HCl (0.1 M). Excess amine will go to aqueous layer. Then the organic layer was washed with brine and dried over anhydrous Na_2SO_4-and filtered, and dried. This modified material, designated as FNI@SiP, was characterized using various techniques including FT-IR, SEM-EDX, TGA, UV-vis spectroscopy and fluorescence spectroscopy.[12]

Fluorescence measurement

For measuring the fluorescence 1g L^{-1} solution of probe is used as stock solution. 20 μL of probe solution was mixed with varying concentrations 0 to 2.7 × 10^{-4} M of picric acid and

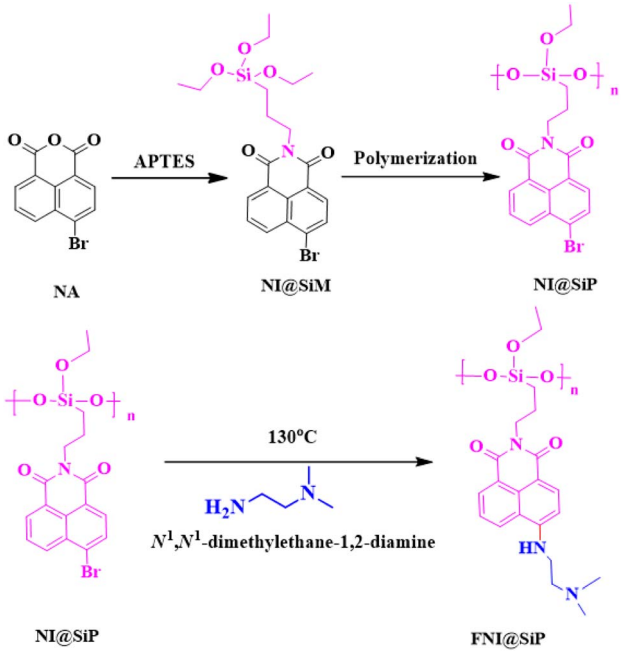

Scheme 1 Scheme for the synthesis of NI@SiP and its functionalization.

made up to 3 mL using deionized water. The measurement was done using fluorescence spectrometer.

Spiking

Real sample analysis was done by spike recovery method. For this, real water samples collected from nearby areas. The water is filtered and pH is corrected using phosphate buffer solution. To this picric acid is added and then the corresponding intensity is measured. From the calibration plot, the concentration is measured.

Lifetime experiment

Life-time decay analyses were performed using solutions of probe with absorbance less than 0.05 by dilution using deionised water. Picric acid added to this with varying concentrations. Decay analyses performed by putting emission maximum wavelength at 500 nm.

Film formation

For the film formation, FNI@SiP dispersed in APTES solution in ethanol (5 mL) was transferred into a Petri dish, covered and kept for the solvent to evaporate at room temperature. A yellowish transparent film was obtained.

Quantum yield determination

The fluorescence quantum yield (Φ_f) of the molecules was determined relative to the reference compound rhodamine B ($\Phi_R = 0.31$ in water) using the provided equation.[15,16]

The quantum yield of the probe was determined using the same method, and the obtained value was used for further analysis.

$$\phi_f = \phi_R \cdot \frac{m_s}{m_R} \frac{{\eta_R}^2}{{\eta_S}^2} \quad (1)$$

Φ_f is quantum yield of the probe; Φ_R is quantum yield of the reference; m_s is slope of integrated area of fluorescence *vs.* Absorbance of probe; m_R is slope of integrated area of fluorescence *vs.* Absorbance of reference; η_R and η_S are refractive indices of solvent used for reference and sample respectively.

Results and discussions

Characterization

Scheme 1 illustrates the synthesis pathway of the polymer NI@SiP and its subsequent functionalization. Characterization of the resulting polymers NI@SiP, and FNI@SiP was conducted using various techniques including FT-IR (Fig. 1).

In the FT-IR spectrum of NA carbonyl stretching bands observed at 1780 and 1730 cm^{-1}. While considering NI@SiP, a new peak is observed at 1660 cm^{-1}, which indicates the formation of the imide structure. The –OH stretching band observed approximately at 3465 cm^{-1} in the case of NI@SiP. Additionally, O–Si–O bands near 950 and 870 cm^{-1} are overlapped by C–O peak. In FNI@SiP, the C–Br peak at 557 cm^{-1} diminished indicating bromine substitution.[17,18]

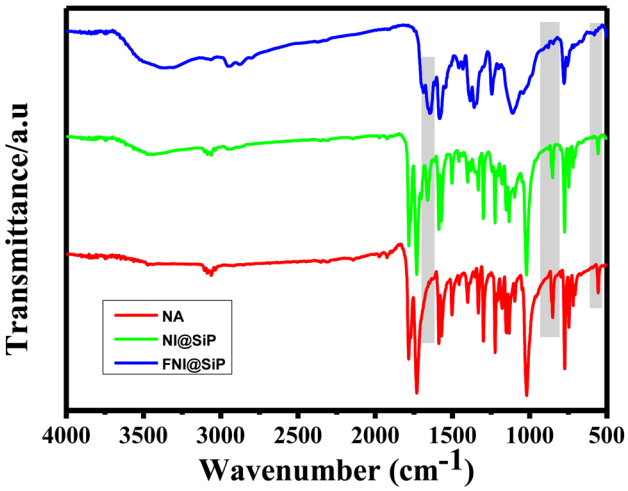

Fig. 1 FT-IR spectrum of NA, NI@SiP, FNi@SiP.

FESEM imaging was employed to investigate the morphological features of the polymer (Fig. 2a and b). Upon functionalization, the FNI@SiP polymer nanoparticles appear to be more detached compared to NI@SiP. FESEM images of APTES is given in Fig. S1. Analysis *via* EDX revealed the presence of C, N, O, Br and Si atoms in the NI@SiP confirming the success of the polymerization process with the desired structure (Fig. 3). Elemental mapping color images are given in Fig. S2a and b shows the corresponding elemental mapping and analysis of FNI@SiP. Comparing both, it is found that upon functionalization the weight percentage of N is increased and that of Br is reduced considerably. This indicate a successful functionalization.

Thermal stability of the NI@SiP, and FNI@SiP was assessed through thermogravimetric analysis (Fig. 4). The minimal weight loss of NI@SIP upto 300 °C, indicates its stability up to 300 °C. This range suggests its potential application in environments where sustained heat resistance is required. The minimal weight loss at lower temperatures underscores its durability and reliability in various operational conditions. Upon functionalization, the TGA curve shows relatively smaller weight loss at lower temperature which could be attributed to the decomposition of the ethylenediamine moiety attached and also the thermal stability of the material was found to be improved.

Photophysical studies of NI@SiP and FNI@SiP

The substitution of alkyl amine at the 4th position of the naphthalimide moiety led to an enhancement in fluorescence

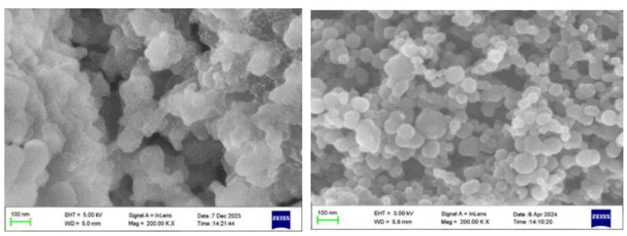

Fig. 2 FE-SEM images of NI@SiP (a, left) and FNI@SiP (b, right).

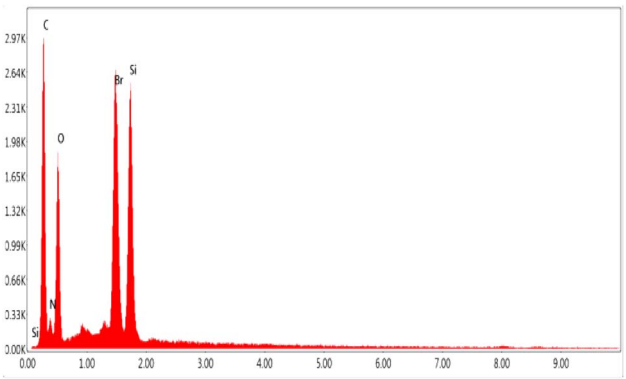

Fig. 3 EDX elemental analysis of NI@SiP.

properties. Furthermore, compared to NI@SiP, the solubility FNi@SiP also witnessed improvement. Absorption and emission properties of the product were explored across various solvents.

The UV-vis absorption spectra of NI@SiP and FNI@SiP solutions in dimethyl formamide (DMF) (6.7 mg L^{-1}) are depicted in the Fig. 5a. NI@SiP exhibited an absorption band spanning the spectral range, from 270 to 380 nm. Conversely, FNI@SiP displayed two absorption bands: one in the UV region at 280 nm and another in the visible region at 431 nm.

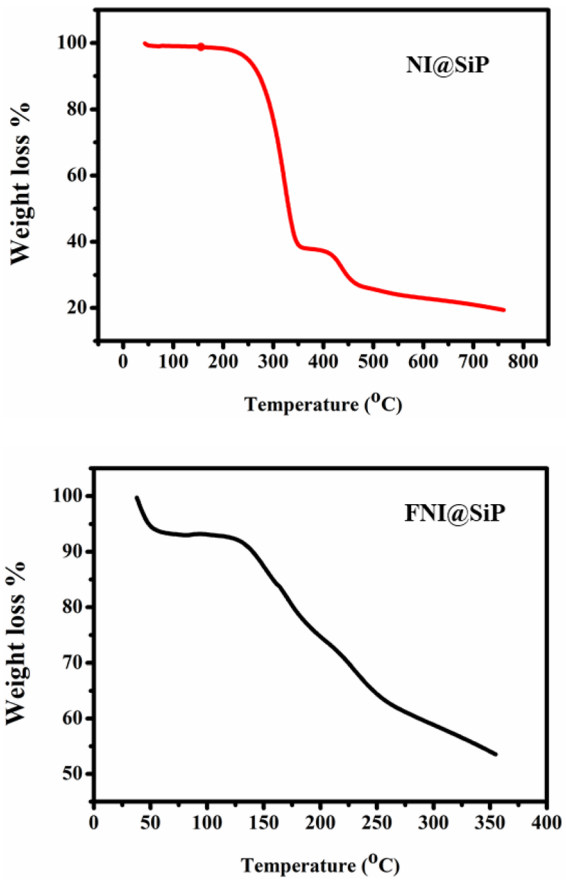

Fig. 4 TGA curves.

Fluorescence emission spectra of NI@SiP and FNI@SiP solutions in DMF were recorded to examine the impact of substituents on their solution fluorescence properties. NI@SiP solution exhibited weak fluorescence signals, whereas FNI@SiP solution displayed significantly stronger fluorescence intensity, substantiating the electronic effect of the substituent on the fluorescence intensity of these compounds in solution.[19] Fluorescence emission spectra of NI@SiP and FNI@SiP solutions in DMF were recorded to examine the impact of substituents on their solution fluorescence properties.

By coupling 4-bromo-1,8-naphthalic anhydride (NA) with the coupling agent APTES, NA could be incorporated into the polysiloxane system *via* chemical linkage. The resulting hybrid samples (NI@SiP) are capable of forming homogeneous and transparent membranes on glass or certain plastic substrates.[19] Typically, 1,8-naphthalic anhydride derivatives bearing electron-withdrawing groups exhibit weak emission. However, photographs of FNI@SiP display strong fluorescence, suggesting that the functionalization of the naphthalic anhydride in our experiments improved the fluorescence properties.

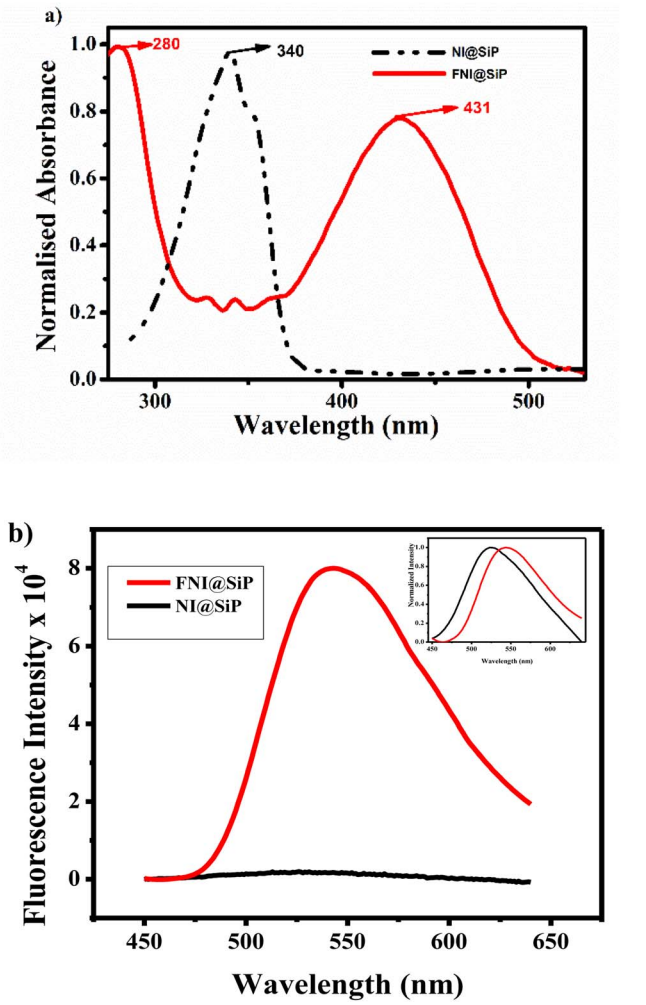

Fig. 5 (a) UV-vis absorption spectra of and NI@SiP and FNI@SiP in DMF (b) fluorescence spectra (λ_{ex} = 430 nm) of NI@SiP and FNI@SiP in DMF (6.7 mg L^{-1}) (inset shows normalized emission spectrum).

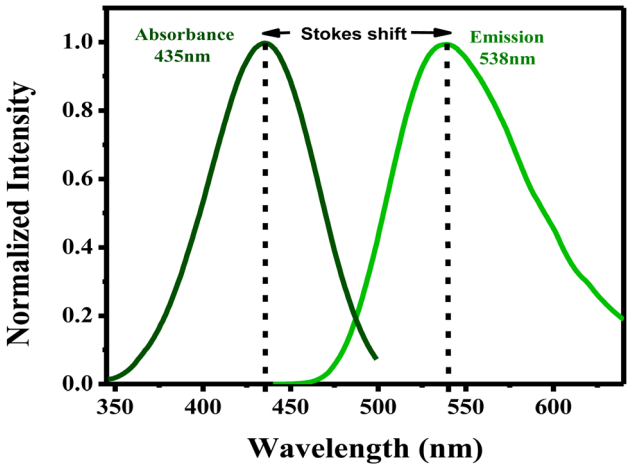

Fig. 6 Excitation and emission spectrum of the FNI@SiP in water.

As discussed previously, NA exhibits weak fluorescence when dissolved in DMF, whereas NI@SiP demonstrates improved emission. With the synthesis of FNI@SiP, which features an electron-donating substituent, the objective was to further enhance fluorescence intensity. Indeed, the fluorescence intensity of FNI@SiP solution significantly surpassed that of NI@SiP solution as shown in Fig. 5b. In addition to this, the final product demonstrated improved solubility in various solvents compared to NI@SiP.

The increased fluorescence intensity of NI@SiP compared to NA can be attributed to several factors. When NA molecules are chemically bonded to the polysiloxane, the chromophores become fixed within the inorganic network, potentially limiting their mobility due to the rigid Si–O–Si network.

The absorption spectra in dimethylformamide (DMF) solution reveal a bathochromic shift with the longer wavelength absorption for FNI@SiP compared to NI@SiP. This shift is likely attributed to the electron-donating abilities of *N*,*N*-dimethylethylenediamine at the C-4 position of 1,8-naphthalimide.

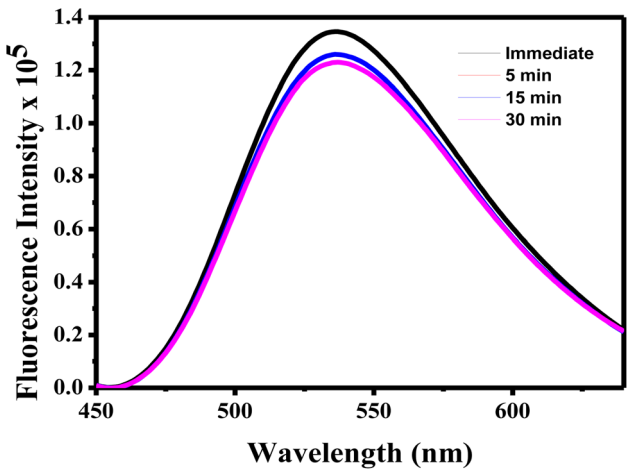

Fig. 7 Time-dependent emission spectra of FNI@SiP (6.7 mg L^{-1} in dI water, λ_{ex} = 430 nm) upon continuous illumination upto 30 minutes.

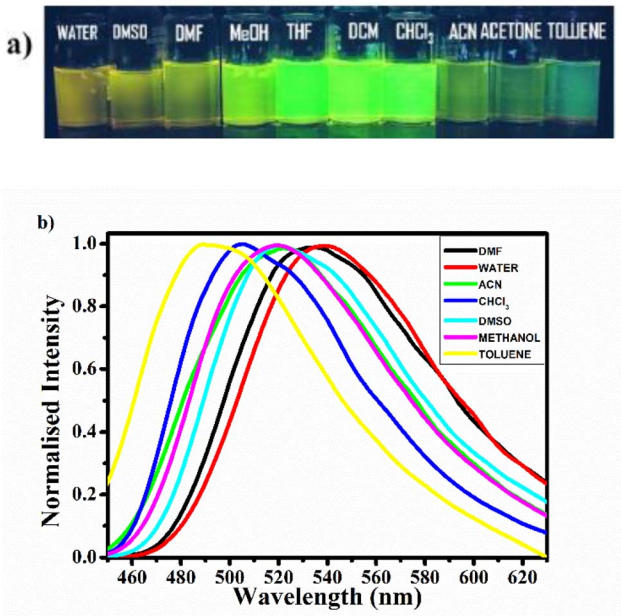

Fig. 8 (a) Solvatochromism (b) normalized emission spectra of FNI@SiP in various solvents (6.7 mg L^{-1} in dI water, λ_{ex} = 430 nm).

The Stokes shift (Fig. 6), indicates the difference in properties and structure of fluorophores between the ground state S_0 and the first excited state S_1.[16]

Mathematically, it can be expressed as (eqn (2))

$$\text{Stokes shift} = \lambda_{\text{emission}} - \lambda_{\text{absorption}} \quad (2)$$

The Stokes shift of this compound obtained is 103 nm.

Photo stability

Photo stability of fluorescent polymers refers to their ability to maintain their fluorescence intensity and emission characteristics when exposed to light, particularly under prolonged irradiation. FNI@SiP is found to be quite stable under prolonged irradiation of light for about 30 minutes without much decrease in its fluorescence intensity (Fig. 7).

Quantum yield

The quantum yield of the probe FNI@SiP was calculated using eqn (1). For this, absorbance and integrated fluorescence

Table 1 Variation of Stoke's shift on the volume fraction of acetonitrile

Volume fraction of acetonitrile	Absorption maxima	Emission maxima	Stoke's shift cm^{-1}	Solvent polarity parameter
0	430	513	3762	0.136
20	427	523	4299	0.318
40	427	529	4516	0.389
50	427	532	4622	0.397
60	427	536	4762	0.422
80	427	541	4935	0.455

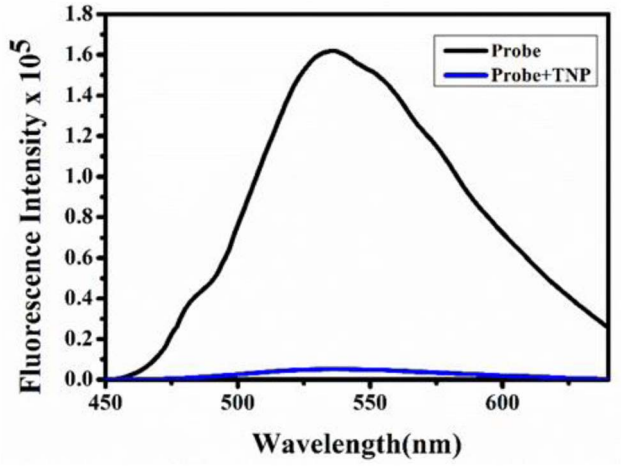

Fig. 9 Fluorescence spectra of the FNI@SiP (6.7 mg L^{-1} in dI water, λ_{ex} = 430 nm) in the absence and presence of TNP.

intensity of FNI@SiP and rhodamine B was measured. The fluorescent measurement was carried out at an excitation wavelength of 500 nm, since both compounds exhibited overlapping absorbance at this wavelength. Absorbance was kept below 0.1 to avoid innerfilter effects. From the plot of absorbance *vs.* integrated fluorescence intensity given in Fig. S5, the quantum yield of FNI@SiP is calculated to be 23.3%.

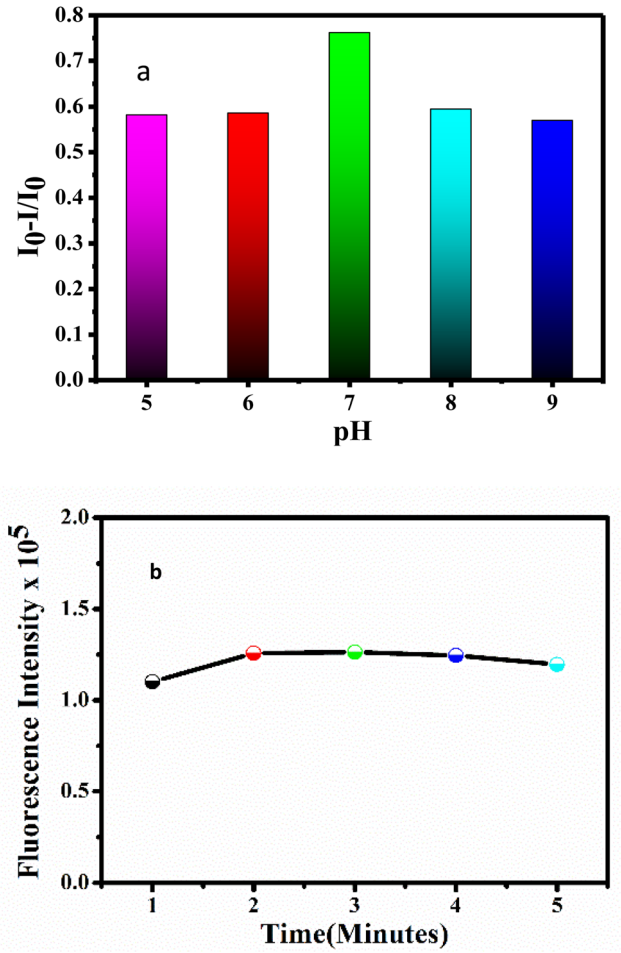

Fig. 10 (a) pH dependence on the quenching efficiency of FNI@SiP (b) fluorescence quenching response time of FNI@SiP towards TNP.

Solvatochromism

FNI@SiP dispersion exhibits yellow-green fluorescence under UV illumination in various solvents, attributed to charge transfer in the 1,8-naphthalimide moieties from the electron-donating alkyl amino group at the C-4 position to the carbonyl groups. The fluorescence emission, observed in the visible region, features pronounced maxima at 490–550 nm, with a bathochromic shift in emission maxima as solvent polarity increases (Fig. 8). The fluorescence curve mirrors the absorption spectrum, indicating preservation of the fluorophore molecular structure in the excited state.

For further understanding the charge transfer characteristics of the polymer, solvatochromic experiments were carried out by varying the polarity of the solvent. For this purpose, a solvent mixture of acetonitrile and toluene with varying ratio were prepared followed by measuring the absorption and emission spectra of the polymer in this solvent mixtures. Fig. S3a shows the absorption spectra of the FNI@SiP in various solvents. It indicates that absorption has not much dependance on the solvent polarity, while emission spectra (Fig. 8b) show a gradual redshift with increase in polarity of the solvent mixture. Thus, it infers that the dipole moment of the excited state is higher compared to the ground state. The increase in Stoke's shift of the polymer with increase in solvent polarity is also evident from the figure. The corresponding absorbance and emission graph of the FNI@SiP in solvent mixture of acetonitrile:DMF mixture of varying ratio also given (Fig. S3b and c respectively). Table 1 shows the variation of Stoke's shift with difference in the volume fraction of acetonitrile. Solvent polarity parameter is used to evaluate the polarity of the solvent mixtures. The value of solvent polarity parameter was obtained from literatures. A plot of solvent polarity parameter against Stoke's shift is given in Fig. S4. The linear relation shows the excited state is more polar compared to the ground state. This may increase the stability of the excited state in polar environment and therefore it can be a reason for absence of excited state interaction between TNP and the FNI@SiP.

Optimization of parameters

In the presence of TNP, fluorescence of the probe, FNI@SiP was found to be decreasing as shown in Fig. 9.[5,20] Fluorescence emission spectra of the dyes as a function of pH were recorded in PBS (pH 5–9) and the quenching efficiency is plotted as a function of pH in Fig. 10a. Upon decreasing pH, the quenching efficiency was found to be decreasing. The pH was optimized by considering the quenching efficiency of the FNI@SiP at different pH, in the presence of a particular concentration of the analyte. It was found that pH 7 gives the best quenching towards the analyte. The response time was checked by monitoring the fluorescence signal of FNI@SiP in presence of the analyte at different time intervals and it was found that the fluorescence signal was stable from two

minutes onwards, which was taken as the optimum response time (Fig. 10b).

Analytical studies

In the analytical studies towards sensing of nitroaromatics, FNI@SiP demonstrated efficient detection capability in aqueous solution. Fluorescent titration revealed a decrease in emission intensity with incremental addition of TNP in the range of 0 to 2.7×10^{-4} M (Fig. 11a). The calibration plot (Fig. 11b) shows a linear relation, in the range, 1.7×10^{-6} M to 2.7×10^{-4} M with equation, $y = -536.65x + 126\,725$, and R^2 0.97. The limit of detection (LOD) was determined using the equation LOD $= 3\sigma/S$, where σ is the standard deviation of fluorophore emission intensity in the absence of an analyte, and S is the slope of the calibration curve.

The overall sensing process is schematically represented below (Scheme 2). The film formed on the solid substrate under visible and UV light (365 nm) is shown in photograph (a and b). TNP solution is used to manually write on the film, and the fluorescence in that written area is significantly lost, which is clearly evident. This visual effect can be utilized for real-world applications.

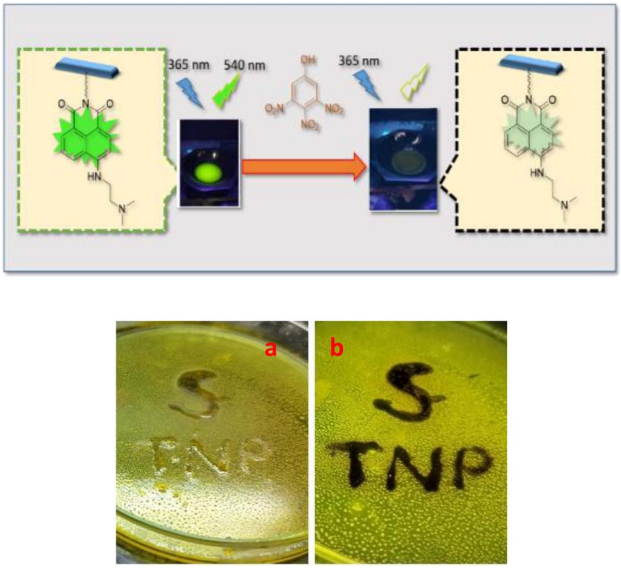

Scheme 2 Scheme for the fluorescent sensing towards TNP. Photograph (a) film written with TNP under visible light (b) film written with TNP under UV light.

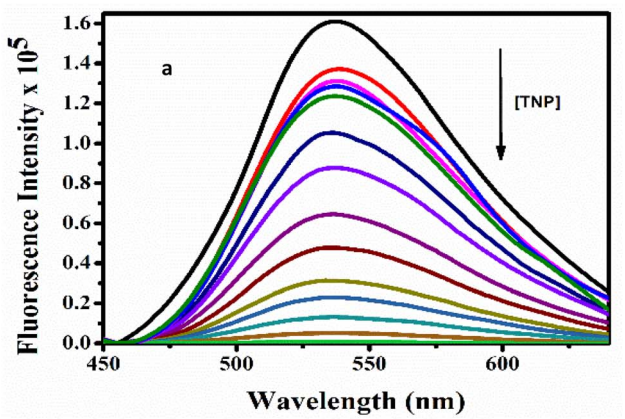

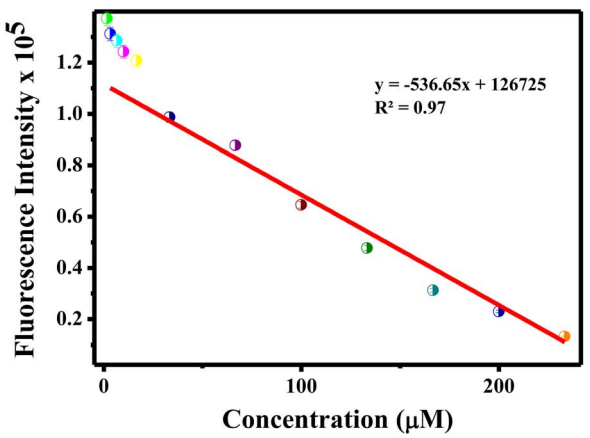

Fig. 11 (a, Top) Fluorescence spectra of the FNI@SiP with incremental addition of TNP and (b. bottom) calibration plot.

Mechanism analysis

S–V plot the fluorescence quenching mechanism was examined and quantified using the Stern–Volmer (SV) equation, which describes the relationship between the fluorescence intensities in the absence (F_0) and presence (F) of a quencher, represented by the quencher concentration ([Q]). The SV plot (Fig. 12) displayed deviation from linearity within the concentration range of 1.7×10^{-6} to 2.7×10^{-4} M, indicating the presence of more than one mechanism.

To analyze the data, polynomial fitting was employed according to the equation $y = 0.0000017x^3 - 0.00032x^2 + 0.029x$ ($R^2 = 0.99$). The non-linearity indicates the possibility of a combination of mechanism in the quenching process.

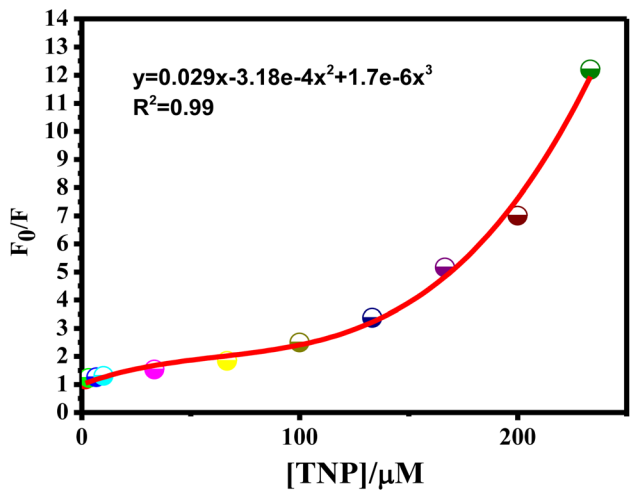

Fig. 12 Polynomial fitting of a non-linear S–V plot of FNI@SiP using TNP as quencher.

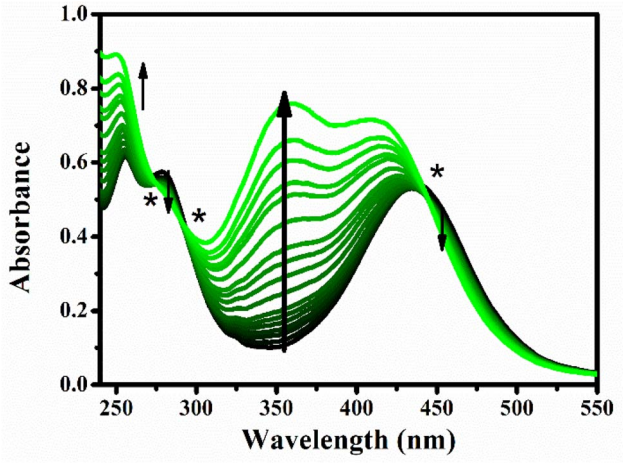

Fig. 13 UV-vis absorption titration spectra of FNI@SiP with TNP in water.

Absorption study. To confirm the quenching mechanism, UV-visible titration (Fig. 13) of FNI@SiP with TNP was conducted. The absorption peak of FNI@SiP near 430 nm shifted towards lower wavelength with increasing TNP concentration, accompanied by the emergence of a new peak near 350 nm. The corresponding calibration plot exhibited a linear relationship in the concentration range of 0–33.3 μM.

UV-visible absorption spectra of FNI@SiP in the presence of increasing concentration of TNP exhibits isobestic points, with increase in absorbance near 450 nm and 300 nm confirming ground state interaction between TNP and FNI@SiP.

Lifetime decay analysis. Fluorescence quenching necessitates molecular contact between the fluorophore and the quencher, which can occur through complex formation (static quenching) or diffusive encounter (dynamic quenching). Time-resolved measurement of fluorescence decay can distinguish between these processes. In static quenching, non-fluorescent fluorophore–quencher complexes are formed, leaving the fluorophore's lifetime unchanged with increasing quencher concentration. In dynamic quenching, collisional encounters between the quencher and the excited fluorophore result in a decrease in the average fluorescence lifetime.

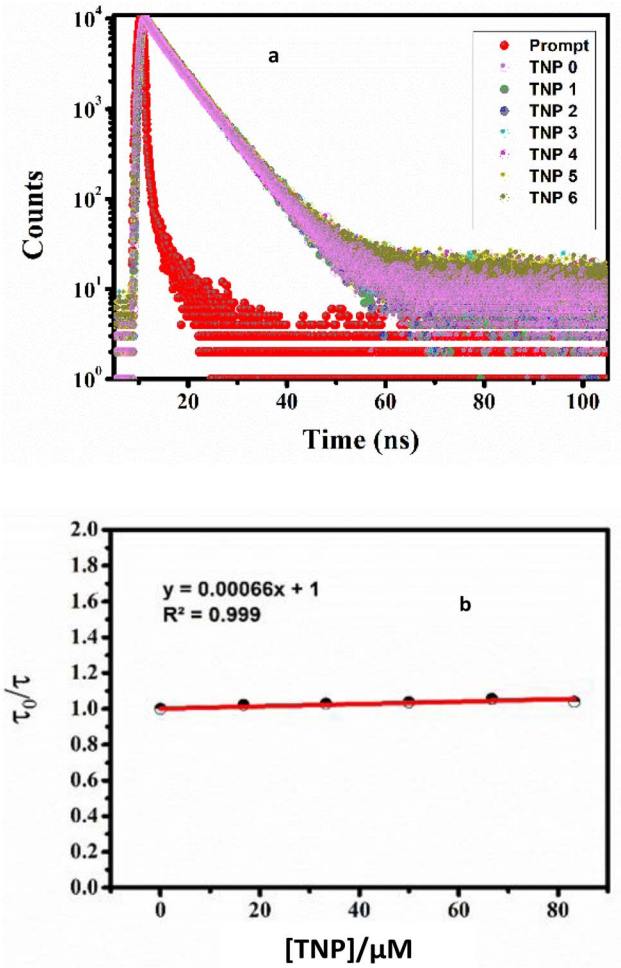

Fig. 14 (a) Time resolved life time decay curves for FNI@SiP with addition of TNP (b) calibration.

The decay processes exhibited an average lifetime of 4.6 ns for FNI@SiP (Fig. 14a). Upon the addition of TNP, the average lifetime showed no considerable change, indicating that there is no excited state interaction between the fluorophore and TNP (Fig. 14b). But the mechanism involves more than one mechanism as observed by the non-linearity in the Stern–Volmer plot for TNP. The signal of ground state complex formation in the

Table 2 Shows recent literature reports on fluorescent polymer-based sensors towards TNP

Probe	Mechanism	Features	Reference
Conjugated polyfluorenes PF1, PF2	IFE	K_{sv} 5.1 × 10^4 M^{-1} and 5.0 × 10^4 M^{-1} LOD-110 (PF1), 219 nM (PF2)	20
A cationic conjugated polyelectrolyte	PET, RET	K_{sv} 1.12 × 10^8 M^{-1} LOD 30.9 pM	2
A polyfluorene derivative	IFE, PET	K_{sv} 1.05 × 10^5 M^{-1} LOD 57.8 nM	3
Alanine based dansyl tagged copolymer	PET	K_{sv} 1.6 × 10^3 M^{-1} (TNP) LOD not mentioned	21
P(MMA-*co*-TCMA)–copolymer	FRET	K_{sv}-0.259 × 10^4 M^{-1} (DNT), 1.399 × 10^4 M^{-1} (TNT) LOD not mentioned	22
FNI@SiP	IFE, charge transfer complex	Non-linear S–V plot LOD 26.3 nM	This work

UV-vis spectra of the fluorophore, resulting from perturbation by the analyte, reflects the possibility of static quenching.

The lifetime decay was fitted using the equation $y = 0.00066x + 1$, which corresponds to the equation (eqn (3))

$$\frac{\tau_0}{\tau} = K_D[Q] + 1 \quad (3)$$

where τ_0 is the average lifetime of the polymer in the absence of an analyte, τ is the average lifetime in the presence of the analyte, and K_D is the dynamic quenching constant. The value of K_D obtained from the graph is only 6.6×10^{-10} M^{-1}. The very small value of the dynamic quenching constant indicates that the mechanism involves static quenching to a considerably higher extent than dynamic quenching. Table 2 shows recent literature reports on fluorescent polymer-based sensors towards TNP.

To determine the static quenching constant, the apparent quenching constant, K_{app} was plotted against $[Q]$. According to the equation (eqn (4))

$$\frac{F_0}{F} = 1 + K_{app}[Q] \quad (4)$$

$$K_{app} = \left[\frac{F_0}{F} - 1\right]\frac{1}{[Q]} = K_D + K_S + K_S K_D[Q] \quad (5)$$

where, the apparent quenching constant was calculated at different quencher concentration and the plot of K_{app} *versus* $[Q]$ (eqn (5) and Fig. S6) yielded a straight line with an intercept (I) of $K_D + K_S$ and a slope (S) of $K_S K_D$. By solving the quadratic equation $K_S^2 + K_S I + S = 0$, where I is the intercept of the plot and S is the slope. The individual values of K_S were determined to be 1.25×10^4 and 1.07×10^{-12}. Given that static quenching is more pronounced in the mechanism, the value of K_S was determined to be 1.25×10^4 M^{-1}.

FRET. FRET possibility was checked by analysing the absorbance spectrum of TNP and emission spectrum of fluorophore given in Fig. 15. The negligible overlap between the spectra confirms the absence of FRET.[23]

Inner filter effect (IFE). The inner filter effect acts as a quenching mechanism in fluorescence spectroscopy by absorbing either the excitation light or the emitted fluorescence light, thereby reducing the observed fluorescence intensity.[24–28] The presence of inner filter effect in the quenching process can be identified by plotting, absorbance of the quencher with absorbance or emission of the probe. Here, there is significant

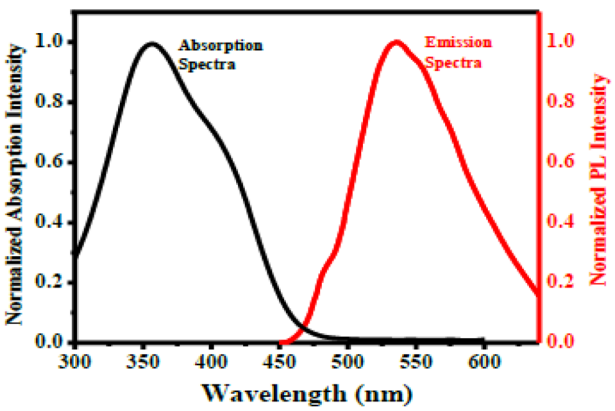

Fig. 15 Absorption spectrum of the analyte and emission spectrum of FNI@SiP (λ_{ex} = 430 nm, in water).

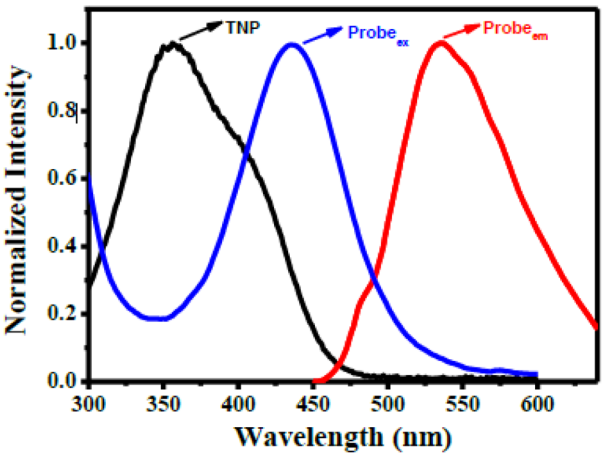

Fig. 16 Absorption spectrum of the TNP, absorption spectrum of the FNI@SiP and emission spectrum of the FNI@SiP.

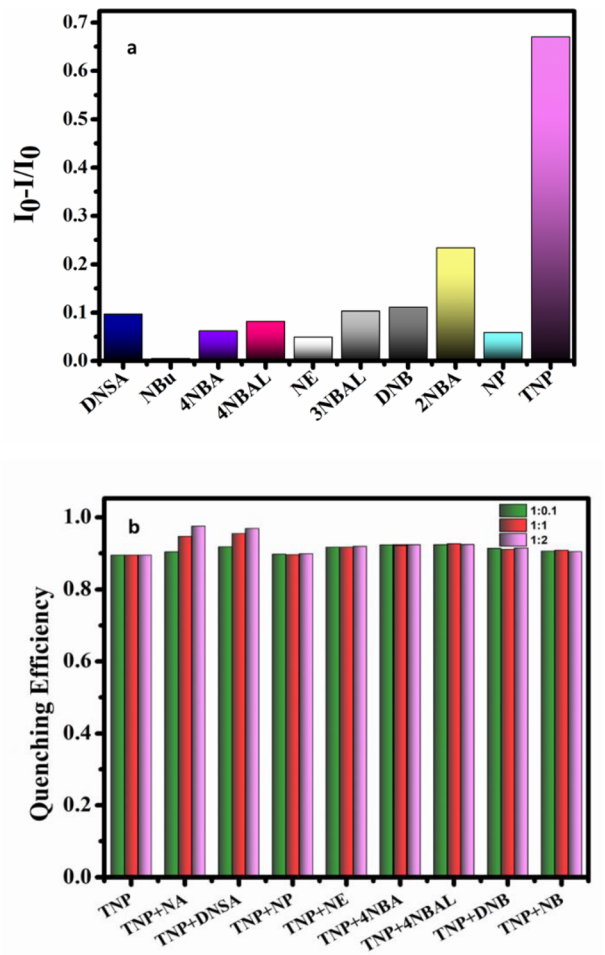

Fig. 17 (a) Fluorescence quenching efficiency of various nitro group containing specie (b) interference of nitro group containing specie on the quenching efficiency of TNP (colour bars indicate ratio of TNP and interferent 1 : 0.1, 1 : 1, 1 : 2 respectively).

Table 3 Real sample analysis

Sample	TNP added (μM)	Found concentration (μM)	Recovery percentage	RSD (%) ($n = 3$)
Well water	4.00	4.29	107.30	3.5
	15.0	14.4	96.00	3.0
	25.0	23.6	94.40	3.4
Tap water	4.00	3.50	87.50	4.1
	15.0	13.0	86.70	3.2
	25.0	23.0	92.00	3.6

overlap between the absorbance of TNP and absorbance of FNI@SiP (Fig. 16) indicating a primary innerfilter effect involved in the quenching process.[28]

Selectivity and interference. The selectivity of the probe was analysed using other nitroaromatics as well as some nitro group containing molecules. DNSA – dinitrosalicylaldehyde, NP – nitrophenol, NE – nitroethane, 4NBA – 4-nitrobenzoic acid, 4NBAL – 4-nitrobenzaldehyde, DNB – dinitrobenzene, and NB – nitrobenzene were used for the study. The quenching efficiency was plotted against these molecules in Fig. 17a, which shows that the probe, FNI@SIP is selective towards TNP.

The interference studies were carried out by measuring the quenching efficiency of FNI@SiP towards TNP in the presence of other species in different ratios. The results obtained is given in Fig. 17b. The material is found to be selective towards TNP with negligible interference from other similar specie.

Real sample analysis. Real water sample analysis was carried out by spike recovery method. Water samples collected from nearby industrial area was filtered to remove bigger particles. The pH of samples was corrected using phosphate buffer solution. After spiking it with different concentrations of TNP, it was analyzed by fluorescence spectroscopy. The corresponding data is tabulated in Table 3. The recovery percentage obtained is between 107.3 and 86.7 with relative standard deviation less than 5%.

Conclusions

A naphthalimide appended APTES polymer, FNI@SIP was synthesized and functionalized for fluorescent sensing application. It was used towards the sensing of TNP in aqueous media with linear response from 1.7×10^{-6} M to 2.7×10^{-4} M with LOD as 26.3 nM. Overall mechanism of the quenching process involves inner-filter effect as well as ground state charge transfer complex formation. The sensor shows reproducible results and it was successfully used towards the sensing of TNP in real water samples by spike recovery method. A thin film was fabricated using APTES which exhibited notable fluorescent quenching upon exposure to TNP. The visual detection patterns under UV light can be used for practical sensing and security applications.

Author contributions

Kala R., conceptualisation, visualisation, supervision, validation, project administration, funding acquisition, resources, review and editing. Sithara Soman: conceptualisation, formal analysis, investigation, visualisation, writing original draft.

Conflicts of interest

There are no conflicts to declare.

Data availability

The data supporting this article have been included as part of the supplementary information (SI). Supplementary information is available. See DOI: https://doi.org/10.1039/d5ra03588k.

Acknowledgements

The authors thank Cochin University of Science and Technology (CUSAT). We thank DST-SERB (EMR/2016/005601), DST-FIST & PURSE, UGC-SAP, PLEASE (Performance Linked Encouragement for Academic Studies and Endeavours) -Establishment of centre for sensor Devices (P3/24770/2020/DCE) under Govt. of Kerala, CUSAT-SMNRI (Seed Money for New Research Initiatives) and RUSA Major projects for financial support, and SAIF-STIC, DOP CUSAT, ISP CUSAT, AIMS(Kochi) for analytical facilities.

References

1 S. Dhiman, N. Singla, M. Ahmad, P. Singh and S. Kumar, *Mater. Adv.*, 2021, **2**, 6466–6498.
2 V. Kumar, B. Maiti, M. K. Chini, P. De and S. Satapathi, *Sci. Rep.*, 2019, **9**, 7269.
3 P. Taya, B. Maiti, V. Kumar, P. De and S. Satapathi, *Sens. Actuators, B*, 2018, **255**, 2628–2634.
4 S. Nath, S. K. Pathak, B. Pradhan, R. K. Gupta, K. A. Reddy, G. Krishnamoorthy and A. S. Achalkumar, *New J. Chem.*, 2018, **42**, 5382–5394.
5 S. Kaja, D. P. Damera and A. Nag, *Anal. Chim. Acta*, 2020, **1129**, 12–23.
6 B. The Huy, D. T. Thangadurai, M. Sharipov, N. Ngoc Nghia, N. Van Cuong and Y. I. Lee, Elsevier Inc., 2022, DOI: 10.1016/j.microc.2022.107511.
7 L. Roos, F. P. Malan and M. Landman, Elsevier B.V., 2021, DOI: 10.1016/j.ccr.2021.214201.
8 J. F. Zhang, M. Park, W. X. Ren, Y. Kim, S. J. Kim, J. H. Jung and J. S. Kim, *Chem. Commun.*, 2011, **47**, 3568–3570.
9 C. Mei, G. Tu, Q. Zhou, Y. Cheng, Z. Xie, D. Ma, Y. Geng and L. Wang, *Polymer (Guildf.)*, 2006, **47**, 4976–4984.
10 A. Kriltz, C. Löser, G. J. Mohr and S. Trupp, *J. Sol. Gel Sci. Technol.*, 2012, **63**, 23–29.
11 E. B. Veale, G. M. Tocci, F. M. Pfeffer, P. E. Kruger and T. Gunnlaugsson, *Org. Biomol. Chem.*, 2009, **7**, 3447–3454.
12 R. Parkesh, T. C. Lee and T. Gunnlaugsson, *Org. Biomol. Chem.*, 2007, **5**, 310–317.
13 S. Çulhaoğlu, F. Kolcu and İ. Kaya, *React. Funct. Polym.*, 2021, **166**, 104978.
14 J. Bujdák, M. Danko, D. Chorvát, A. Czímerová, J. Sýkora and K. Lang, *Appl. Clay Sci.*, 2012, **65–66**, 152–157.

15 E. R. Triboni, C. C. S. Cavalheiro, M. J. Politi, M. P. Bemquerer and M. A. Rodrigues, *J. Photochem. Photobiol., A*, 2010, **208**, 36–41.
16 C. Würth, M. Grabolle, J. Pauli, M. Spieles and U. Resch-Genger, *Nat. Protoc.*, 2013, **8**, 1535–1550.
17 J. R. Lakowicz, *Principles of Fluorescence Spectroscopy*, 2006.
18 A. S. Tanwar, S. Patidar, S. Ahirwar, S. Dehingia and P. K. Iyer, *Analyst*, 2019, **144**, 669–676.
19 H. Khanjanzadeh, R. Behrooz, N. Bahramifar, W. Gindl-Altmutter, M. Bacher, M. Edler and T. Griesser, *Int. J. Biol. Macromol.*, 2018, **106**, 1288–1296.
20 A. H. Malik, S. Hussain, A. Kalita and P. K. Iyer, *ACS Appl. Mater. Interfaces*, 2015, **7**, 26968–26976.
21 A. S. Tanwar, S. Hussain, A. H. Malik, M. A. Afroz and P. K. Iyer, *ACS Sens.*, 2016, **1**, 1070–1077.
22 F. D. J. Trindade, E. R. Triboni, B. Castanheira and S. Brochsztain, *J. Phys. Chem. C*, 2015, **119**, 26989–26998.
23 P Keerthana, A. R. Cherian, U. Sirimahachai, D. A. Thadathil, A. Varghese and G. Hegde, *J. Environ. Chem. Eng.*, 2022, **10**, 2.
24 H. Li, B. Fu, W. Yang, L. Ding, Y. Yang, J. Dong, F. Wang and Q. Pan, *Spectrochim. Acta, Part A*, 2020, **226**, 117575.
25 K. Shanmugaraj and S. A. John, *New J. Chem.*, 2018, **42**, 7223–7229.
26 A. Kathiravan, M. Narayanan, M. Asha Jhonsi and V. Anbazhagan, *Spectrochim. Acta, Part A*, 2023, **303**, 123166.
27 A. S. Tanwar, R. Parui, R. Garai, M. A. Chanu and P. K. Iyer, *ACS Meas. Sci. Au*, 2022, **2**, 23–30.
28 A. S. Tanwar, S. Patidar, S. Ahirwar, S. Dehingia and P. Krishnan Iyer, *Analyst*, 2019, **144**, 669–676.